Surfaces and Interfaces 31 (2022) 102048

Contents lists available at ScienceDirect

Surfaces and Interfaces

journal homepage: www.sciencedirect.com/journal/surfaces-and-interfaces

Thermal annealing of natural rubber films controls wettability and enhances cytocompatibility

Rodney Marcelo do Nascimento [a,b,*], João Elias F.S. Rodrigues [c], Bruno Z. Favarin [d], Ana P. Ramos [d], Pietro Ciancaglini [d], Carlos Pecharroman [c], Rachid Rahouadj [e], Antônio Carlos Hernandes [b], Ivan Helmuth Bechtold [a,*]

[a] Physics Department, Federal University of Santa Catarina, 88040-900 Florianópolis, SC, Brazil
[b] Institute of Physics, University of São Paulo, 13566-590, São Carlos, SP, Brazil
[c] Instituto de Ciencia de Materiales de Madrid (ICMM), Consejo Superior de Investigaciones Científicas (CSIC), Sor Juana Inés de la Cruz 3, E-28049 Madrid, Spain
[d] Department of Chemistry- FFCLRP- University of São Paulo, Ribeirão Preto-SP Brazil
[e] Laboratoire d'Etude des Microstructures, de Mécanique des Matériaux et du Vivant, LEM3 UMR CNRS 7239, University of Lorraine Nancy-Metz, 57070, France

ARTICLE INFO

Keywords:
Natural rubber
Thermal treatment
Wettability
Surface energy
Cytocompatibility

ABSTRACT

In spite of the widespread use of natural rubber in regenerative therapies, thermally induced modifications of its complex chemical structure and their effect on the surface properties and the cell response (attachment-adhesion-proliferation) are still an unexplored topic. Here, we demonstrate how thermal treatments enhance the cell response due to changes to the inner and surface structures of natural rubber. *In situ* studies of the temperature effects conducted via infrared spectroscopy revealed both molecular rearrangements and anharmonic effects in the polymeric lattices. Thermal treatments at different temperatures allowed to control the wetting regime. Contributions of different surface parameters to the wettability were decoupled by statistical analysis of the principal component. The polar component of the surface free energy was recognized as the main surface player, which influences cell spreading, attachment, proliferation, and tissue growth. A simple thermal annealing of the natural rubber film at 373 K alters the local structure of the latex inducing an increase in cell viability. The experimental-statistical analysis approach allows an accurate correlation of physicochemical properties with cell supportability. The results highlight the potential of natural rubber polymers by tuning surface wettability, via simple thermal treatment, for biomedical applications.

1. Introduction

Over the past years, natural rubber (NR)-based materials extracted from *hevea brasiliensis* trees have become protagonists in research aiming at medical applications [1–8]. Some of the NR properties and applications that are of interest at the interface of biomedical sciences and engineering include its antimicrobial behavior [9], reinforcements for anthropomorphic prosthetics [10], its ability to encapsulate bioceramics [11], the formation of apatites in contact with biological fluids [12], and the modulation of surface charges and the adsorption of blood components [13]. The material can be processed as a type of composite stem cell that favors cartilage formation [14], in addition to acting as flexible cell support to guide cell membrane changes [15]. The notable properties that enable such applications are due to the isoprene matrix of the rubber and non-rubber particles naturally present in the material. Recently, the biomedical applications of NR have been reviewed in detail [16].

Understanding the relationship between surface physicochemical properties and cell responses entails wide possibilities for the rational design of functional biomaterials, i.e., the correlation of surface wettability (SW) and cell viability that impacts graft integration and tissue regeneration following implantation [17–19]. This physicochemical parameter is measurable by the contact angle (θ) formed between a liquid droplet and a testing surface. However, SW is not an independent variable: it is a result of other physicochemical parameters, such as topography [20] and surface free energy [21]. NR surfaces are hydrophobic, with $\theta \approx 90^{\circ}$ [12]. The surface free energy (SE), as well as its dispersive and polar components, can be tuned by removing or adding specific components. For instance, the polar component of the SE of latex films can be decreased by deproteinization [22], while the increase

* Corresponding authors.
E-mail addresses: rodney.nascimento79@gmail.com (R. Marcelo do Nascimento), ivan.bechtold@ufsc.br (I.H. Bechtold).

https://doi.org/10.1016/j.surfin.2022.102048
Received 28 January 2022; Received in revised form 2 May 2022; Accepted 11 May 2022
Available online 14 May 2022

of this component can be obtained by the incorporation of polar particles [14].

The possible use of this remarkable material as functional cell support in regenerative medicine or even in fundamental studies of cell phenomenology has attracted great interest in materials science and technology. Nevertheless, as far as we know, thermal modification of its complex chemical structure and the influence on surface properties and cell response (attachment-adhesion-proliferation) has not been explored. A key question is whether thermal treatments may physically (in terms of topology) or chemically (in terms of free energy) affect the SW and, consequently, the cell-material interactions. NR processing using heat treatments may show issues with cytocompatibility properties. From a thermodynamic standpoint, the interfacial interactions between cells and materials result in a localized steady-state (aiming to minimize the free energy of the cell adhesion spreading process), e.g., cells are sensitive to the stability of the surface. On the other hand, NR is susceptible to thermal degradation due to double bonds in the main chain and can affect the stability of the surfaces. On the other hand, the thermal process on polymers varies from solvent to solvent. [23]. Careful choice of heat treatments for polymers melted in solvents must remove the effect of the solvent on cytocompatibility following the control of the surface properties. Assuming that the changes of the SW are directly correlated with the molecular rearrangement, it may be possible to control the wetting of NR only by temperature, thus opening new horizons for NR applications. Physically [24] and chemically [25] adjustable SW is helpful in applied surfaces and interfaces in a wide range of fields, such as decontamination separating oil/water mixtures, waterproofing, self-cleaning, and water collection [26–29]. The chemical rearrangement of the polymeric NR matrices by a pre-thermal treatment could be an easy way to tune NR-SW and thereby the cell-interaction profiles.

This work aims to establish a clear correlation between molecular rearrangement, surface properties, and cell response of NR under thermal treatment. From infrared (IR) in situ analysis, we show how the bulk structure of the NR matrix is changed by temperature. We also address the temperature effect in modulating the surface properties of NR by monitoring wettability by contact angle measurements before and after thermal annealing. A quantitative study employing principal component analysis (PCA) revealed the main player affecting surface wettability. The NR films were then submitted to cell viability assays aiming for biomedical applications. MC3T3-E1 cells (osteoblastic cell line) were seeded on the samples before and after thermal treatments. The temperature-tunable SW on NR, obtained from molecular rearrangements using appropriate thermal treatments, is discussed in view of the physicochemical interactions and their relevant conditions for enhancing cell response. Beyond the fundamental interest of the relations between chemical structure and SW, developing a simple pre-treatment method is of practical interest for applied R&D toward improved NR based-materials.

2. Materials and methods

2.1. Samples

Samples of NR latex were collected from *Hevea brasiliensis* trees (clone RRIM 600) located at Estância Regina farm, São Paulo, Brazil, and the NR films were prepared at Universidade Federal de Santa Catarina, Florianópolis, Brazil. To produce the films, commercial glass substrates of 5 cm^2 were cleaned using an ultrasonic bath with 1. acetone, 2. isopropyl alcohol, and 3. ultrapure water (10 min each) and dried at 40 °C for 10 min. NR aliquots of 1.5 mL were centrifuged during 90 min at 24 °C in an Eppendorf 5418 R centrifuge. After separation, a part of the upper creamy phase was re-dispersed in chloroform until it reached a gel state at room-temperature. A volume of 40 μL of the NR suspensions was carefully dropped on glass substrates using a micropipette and dried at room-temperature for 12 h in a glass desiccator followed by thermal treatment at 333 K during 15 min for solvent elimination. This material processing was defined as "Standard Treatment", labeled ST, and submitted to thermal analysis and in situ infrared spectroscopy investigations from 80 K up to 473 K. The DSC curves represent the first heating process, just after drying according the standard treatment. For the surface property studies (Sections 3.2 and 3.3), the samples were characterized for four additional thermal treatments during 5 min at T1 = 373 K, T2 = 383 K, T3 = 393 K and T4 = 473 K, with heating/cooling rates of ~ 1 °C/min. Samples were prepared in triplicate and, for molecular spectroscopy, contact angle characterization and topography analysis, each one was randomly measured at three distinct positions. Samples were sterilized in UV light for 15 min before the cell culture assays.

2.2. Effect of temperature on NR samples investigated by in situ infrared spectroscopy

NR samples were investigated by *in-situ* Fourier Transform Infrared (FTIR) spectroscopy within a temperature range from 80 to 500 K. FTIR spectra were recorded in a Bruker Hyperion 2000 IR microscope attached to a Vertex 70 V Fourier-transform spectrometer. The light source was a SiC resistance and the beam splitter covered a wide range from 50 to 7000 cm^{-1}. The microscope includes a liquid-nitrogen-cooled MCT detector that was used to record spectra in the range of 4000–1400 cm^{-1} with a resolution of 1 cm^{-1}. The microscope collected light by a Cassegrain 15x objective in reflectance mode. Between the sample and the microscope base, a heater plate, driven by a temperature controller, allowed us to control the temperature with a precision of 1 K. IR background spectra on an aluminum mirror were recorded previously to run 256 successive scans. The obtained reflectance FTIR spectra were converted into Kubelka-Munk approximation and represent the average of spectra acquired at different regions of the sample.

2.3. Atomic force microscopy (AFM)

A Nanosurf FlexAFM microscope was used to determine the surface morphology of the thermally treated NR films. Scanning areas of 25 × 25 μm^2 were captured to estimate the surface roughness parameters under dry conditions. The measurements were done in contact mode using 200 μm, 0.15 N m^{-1} triangular silicon nitride cantilevers with gold-coated tips (OMCL-TR800PSA, Olympus, Japan). Image analyses were performed using the manufacturer's SPM-Offline software (Version 3.304, Shimadzu). The AFM data were treated using the WSxM 5.0 software. Statistical data were obtained from 3 different positions of each sample ($n = 3$). From the surface profiles, the arithmetic average height R_a was calculated concerning the surface amplitude (y), as described by the Eq. (1):

$$R_a = \frac{1}{n}\sum_{i=1}^{n} |y_i| \quad (1)$$

2.4. Contact angle measurements

To evaluate the stability of the wetting regime of the samples, static contact angle (θ) measurements of ultra-pure water droplets (volume ~2 μL) were carried out by the standard sessile drop method on a KSV CAM 200 tensiometer/goniometer. For each experiment, a water drop was deposited on each surface enclosed in a glass chamber. A white and homogeneous light system was positioned behind the sample to make the drop appear black. Side-view drop images were recorded with a CCD camera for subsequent characterization of the hydrophobic/hydrophilic wetting regime of the modified NR films. The temperature around the samples remained at 22 °C ± 2 and the relative humidity was set to 48 ± 6% at the beginning of the experiments.

2.5. Determination of the surface energy

The surface energy of the NR was calculated from the contact angle using liquids with different polarities. At least five measurements were taken in different positions of each sample using water ($\gamma^p = 51$ mN.m^{-1}, $\gamma^d = 21.8$ mN.m^{-1} and $\gamma = 72.8$ mN.m^{-1}), ethylene glycol ($\gamma^p = 19$ mN.m^{-1}, $\gamma^d = 29$ mN.m^{-1} and $\gamma = 48$ mN.m^{-1}) and diiodomethane ($\gamma^p = 0$ mN.m^{-1}, $\gamma^d = 50.8$ mN.m^{-1} and $\gamma = 50.8$ mN.m^{-1}), where γ denotes liquid surface tension and γ^p and γ^d are the polar and dispersive components of γ. The solid surface energy (γ_s) was calculated using the dispersive (γ_l^d) and polar (γ_l^p) components of the liquid surface energy [30]. This method is based on the concept of short and long-range intermolecular interactions, described as polar and dispersive interactions. Thus, γ_s can be obtained from the Young equation substituting the sum of the dispersive γ_S^d and polar γ_S^p components to the total surface energy, as described by Eq. (2):

$$(1+cos\theta)\gamma_i = 2\sqrt{\gamma_l^d\gamma_s^d} + 2\sqrt{\gamma_l^p\gamma_s^p},\ \gamma_s = \gamma_s^d + \gamma_s^p \quad (2)$$

From the linearization of the Eq. (2), we obtain the plot of 0.5 γ (1 + cosθ). $(\gamma^d)^{-1/2}$ versus $(\gamma^p / \gamma^d)^{1/2}$ for the determination of the dispersive γ_S^d and polar γ_S^p yielding γ_S. θ is the contact angle.

2.6. Osteoblast viability determination by optical absorbance

Osteoblast cultures on the NR samples were used to investigate the effects the thermal treatments on the cellular response. The cultures are also useful to investigate the potential cytocompatibility of the NR. Osteoblastic cells MC3T3-E1 (American Type Culture Collection-ATCCt) at first passage were collected in a 75 cm^2 plastic culture flask containing 10 mL of osteogenic culture medium (composed by α-MEM, supplemented with 10 wt.% fetal bovine serum, 1 vol.% penicillin/streptomycin, 5 μg/mL ascorbic acid and 2.16 mg/mL β-glycerophosphate). The cells were cultured until subconfluence was reached, then enzymatically released. First-passage cells were cultured in the same medium, at a concentration of 2×10^4 cells per well, in 24-well microplates (Falcon, Franklin Lakes, NJ, USA), at 37 °C in a humidified atmosphere of 5% CO_2. The cells were cultured with the samples for 48 h. Cell viability was quantified using the standard MTT (3-(4.5-dimethylthiazol-2-yl)−2.5-diphenyl tetrazolium bromide) reduction assay. Formazan production (as an indicator of cellular viability and metabolism) was quantified using an ELISA plate reader in absorbance mode (Multiskan EFLAB, Helsinki, Finland) at 490 nm [31]. Cells cultivated in absence of the materials and cells cultivated on polystyrene discs (in absence of NR) were used as first (100% viability) and second control groups, respectively. The data are reported as the mean ± S.D. of triplicate measurements of different cell cultures.

2.7. Statistical analysis

The results were normally distributed and expressed as the mean ± standard deviation for comparisons, taking $p = < 0.05$ as the threshold for statistical significance. Statistical correlation of each parameter was evaluated by Pearson tests performed by Excell 10 software for multiple comparisons. Statistical significance was evaluated by one-way analyses of variance (ANOVA) and Tukey's honest significant difference (HSD) test for multiple comparisons. For a complete statistical analysis, considering the molecular structure, roughness, wettability surface energy, and cell response, we applied the principal component analysis (PCA) by extracting a set of physical-chemical-biological parameters and converting the data into a data matrix. The dimensionalities were reduced by an alternative set of coordinates in a general format [32], given by:

$$X = TP^T + E \quad (3)$$

where the matrix X is decomposed by PCA into two smaller matrices, T and P, named scores and loadings, respectively. E is the residual of X. The principal component is the linear combination of the original variables, which transform the large number of physical-chemical-biological parameters into a smaller number of uncorrelated variables according to the numerical condition:

$$\sum_{i=1}^{I} t_{ia}t_{ib} = 0; \sum_{i=1}^{I} p_{ia}p_{ib} = 0 \quad (4)$$

where t_a and, t_b are the a^{th} and b^{th} columns of the T matrix, respectively while p_a and p_b are the a^{th} and b^{th} rows of the P matrix. The order of the principal components (PCs) denotes their importance to the spectral dataset. For instance, PC1 described the highest amount of variation, PC2 the second highest, and so on; all PC-loadings were bi-plotted. PCA was performed by Past 3.2 software.

3. Results

3.1. Molecular rearrangement as function of the temperature

We first investigated the thermal stability, mass loss, and percent residue of thermal decomposition of the NR films. The temperature treatments were chosen in a range lower than 473 K, in which significant mass loss was identified, also considering the phase transitions, according to the results from thermogravimetric analysis (TGA) and differential scanning calorimetry (DSC), as depicted in the Figs. 1**(a)** and **1 (b)**, respectively. The annealing temperatures (ST = 333 K, T1 = 373 K, T2 = 383 K, T3 = 393 K and T4 = 473 K) can be better visualized using the vertical dashed lines in the first derivative indicated in Fig. 1**(b)**. At the onset of the transitions, one may observe both exothermic and endothermic associated with protein denaturation and the new chemical phases formation, respectively. Such phase transitions have been assigned to the decomposition of non-rubber components, such as proteins and fatty acids indicating that molecular groups in NR can be quite different before and after the thermal treatments. NR polymeric matrices and their constituents are long-chain molecules of high molecular weight (~10^6 g/mol), and each macromolecular group can be affected differently, depending on the thermal energy. Thus an *in-situ* molecular investigation is required to unravel how the molecular groups and chemical structures are modified within a temperature range.

Infrared spectroscopy analyses were conducted to investigate the chemical composition of the NR samples and the temperature-dependent molecular changes. As displayed in Fig. 2**(a)**, the IR spectra of NR samples depicted the characteristic bands assigned to the macromolecular structures. The complete positions and assignments of bands were also observed in Raman spectra of NR samples and are provided in supplementary tables S1 and S2 in the supporting information. Changes in the profile of the spectra due to the temperature variation were observed. For instance, the enlarged spectra at Fig. 2**(b)** shows changes in the bands ranging from 1500 to 1665 cm^{-1}, assigned to amine and carboxylic groups associated to proteins [33]. In particular, temperature-induced changes at 1541 and 1630 cm^{-1} (amide I and amide II, respectively) are attributed to both, proteins and polypeptides, containing peptide bonds. It is known that the stability of the NR colloidal system is partially rooted in distinct structures of the tryptophan present in the proteins of the NR particles [12]. Temperature changes can affect the conformation of aromatic rings, which in turn modifies the tertiary structure of proteins resulting in a shift of the IR bands. Another striking feature observed in these results is the formation of the new molecular groups, such as C≡C and C≡N bonds, as suggested by the new band present in the 1950–2100 cm^{-1} spectral range with increased temperature, which, according to the DSC characterization, seems to be associated to phase transitions.

Deconvolution of the band between 2800 and 3000 cm^{-1} (compare 343, 373, and 403 K spectra) illustrates displacements in the maximum

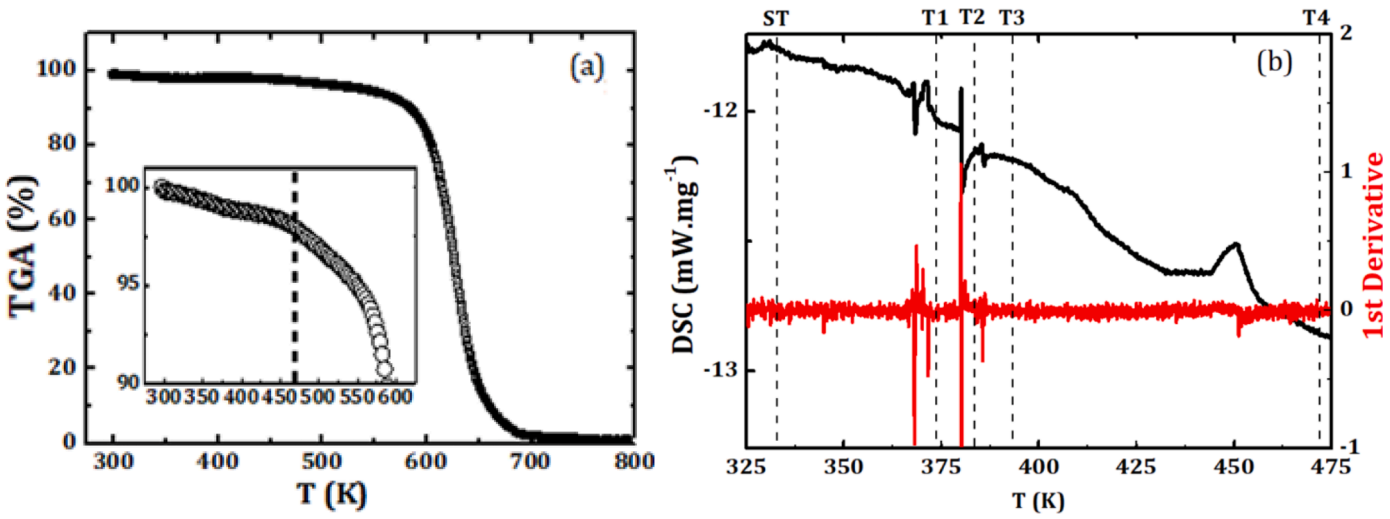

Fig. 1. Results of TGA (a), DSC and its first derivate (b). The dashed lines indicate the temperatures of thermal treatment between different transitions.

of the peaks, see Fig. 2**(c)**. This spectral range is assigned to C—H stretching from CH_2 and CH_3, characteristic of cis-polyisoprene chain groups, as well as, the spectral region of phospholipidic chains characterized by symmetric and antisymmetric stretching modes [34]. This spectral region also exhibits C—H stretching vibrational bands of amino acids, assigned to the presence of protein structures incorporated

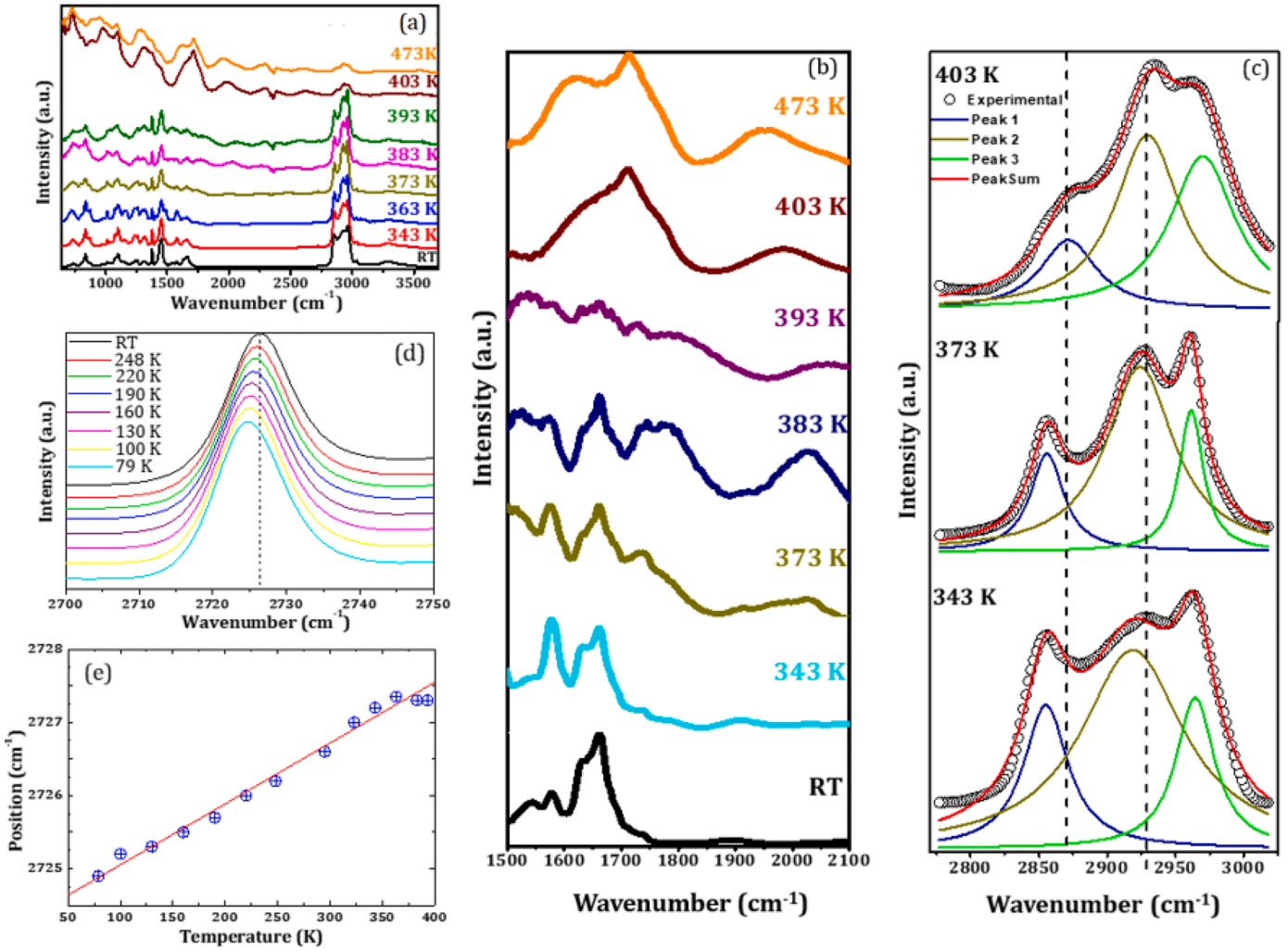

Fig. 2. IR spectra of NR samples obtained at different temperatures showing the modifications in the vibrational spectra from room temperature to higher temperature (a-c) and from room temperature to lower temperature (d). Peak profile analyses of the IR spectra of the 2775–3025 cm^{-1} band regions and peak positions versus temperature of the 2725–2728 cm^{-1} region with linear regression based on the anharmonic temperature-dependent model (e).

in the NR matrix [35].

In addition, the IR spectra revealed a temperature-dependent shift of the peak position in the 2700–2750 cm^{-1} spectral region in Fig. 2**(d)**, attributed to anharmonic effects in the phonon center [36]. This phenomenon can result from several factors in materials physics, such as intrinsic anharmonic contribution, electronic state renormalization, ionic energy change caused by polymeric lattice contraction/expansion, and exchange integral modulation due to the appearance of the magnetic ordering. Here, the anharmonicity of chemical bonds can be a clue to further address the temperature effects on the molecular groups. To support such explanation, we refer to temperature-dependent modeling of the mode position given by a simplified Balkanski model [36], expressed by Eq. (5) where Ω(T) is the peak position as a function of temperature, ν_0 is the vibrational mode in cm^{-1} and C is an adjustable parameter. The multiplier term of C is the anharmonicity constant with $x = hc\nu_0/(2k_bT)$ representing the physical relationship between Planck Constant (h), speed of light (c), Boltzmann Constant (k_b) and Temperature (T).

$$\Omega(T) = \nu_0 + C\left[1 + \frac{2}{e^x - 1}\right] \approx \nu_0 + C\left[1 + \frac{4k_BT}{hc\nu_0}\right] \quad (5)$$

From the fitting using Eq. (5), the following parameter adjustments were obtained for $\nu_0 = 2716$ cm^{-1} and $C = 8.1$ cm^{-1}, having good agreement with the experimental peak positions versus temperature of the 2725–2728 cm^{-1} region, as can be seen in the linear regression of Fig. 1**(e)**. The progressive increase of peak position, with $C > 0$, means that the anharmonicity is an effect of the chemical transition induced by temperature.

An anharmonic potential produces a net displacement of the electronic charge resulting in a modification of the dipoles. It also causes thermal expansion and the anharmonic curve may be associated with the glass transition that the material might experience. However, in a glass transition, modes shift to lower frequencies as temperature increases. A possible explanation is that the polymer tends to change its chemical composition, increasing the tension of the amide bonds so that the material becomes more rigid with temperature until the amides degrade. On the other hand, in a glass transition, the intensity of the mode (concerning a fixed neighbor) is reduced. The irreversible transition around 375 K was also identified by DSC. Near to the transition around 375 K, the peak position started to be constant with temperature. The observed behavior seems to be related to stress around the amide groups, breaking the molecular structure above 375 K. The intensity of the main Raman peaks (2915 cm^{-1} and 1665 cm^{-1}) inverts due to a change of intensity of the C—H stretching signal within the temperature range (see supplementary **Fig. S1**). The probing by IR and Raman spectroscopy of temperature-induced anharmonic effects are imperative in future studies to explore molecular rearrangements in the polymeric matrix. Such results will evidence possible displacements between the positively charged molecular center of mass and the negatively charged electron cloud. This electric dipole moment can result in surface energy modifications, particularly, in its polar component.

3.2. *Effects of the thermal treatments on the surface wettability and surface free energy*

Molecular rearrangement in the polymeric matrix submitted to different temperatures may affect the SW. The θ values for the samples thermally annealed are listed in Table 1. Changes in wetting regimes depending on the thermal treatments can be observed, in particular when water is used as the liquid interface. T1 and T2 increase the NR surface-hydrophilicity compared to ST as indicated by contact angle reduction from $\theta \approx 85°$ to $\theta \approx 70°$ This effect may be caused by changes in topography, surface energy, or both. The contact angles using ethylene glycol (eg) and diiodomethane (di) remain stable in samples submitted to T1 and T2 in comparison to ST.

Table 1
–NR heat treatment temperatures and associated characteristic properties: contact angle values (θ) using water, ethylene glycol (eg) and diiodomethane (di), and AFM-based average roughness (R_a) values measured on NR-samples submitted to different thermal treatments: ST, T1, T2, T3 and T4.

	ST	T1	T2	T3	T4
Temp. (K)	333	373	383	393	473
θ_{water} (°)	85.2 ± 1.2	69.8 ± 1.6	71.4 ± 1.6	99.9 ± 1.4	84.5 ± 3.2
θ_{eg} (°)	80.1 ± 1.8	82.7 ± 3.9	79.0 ± 1.8	97.3 ± 3.8	77.6 ± 5.1
θ_{di} (°)	45.7 ± 1.9	47.3 ± 1.0	49.2 ± 2.7	39.8 ± 3.1	52.5 ± 2.1
R_a (nm)	5.1 ± 2.6	3.9 ± 0.6	5.0 ± 0.9	2.0 ± 0.1	–

A hydrophilic-hydrophobic transition with water is observed between T2 ($\theta \approx 70°$) and T3 ($\theta \approx 100°$). Moreover, a stable wetting regime is obtained after T4 with θ values similar to those obtained on the ST surface. It shows that contact angles can be modulated by molecular rearrangements in the material as a function of thermal treatment.

As mentioned, tunable SW has been considered a key feature for advanced and smart materials. Recently, a study reported the possibility to tune hydrophobicity of NR by incorporating silica [37]. However, such a procedure inevitably modifies the inner structure and morphological properties of the NR making the natural polymer a composite. Our results reveal that the wetting of the NR can be tuned by simple thermal annealing without incorporation of any other dopants.

As aforementioned, SW depends on other physicochemical properties, such as surface topography and free energy. Since ST and T4 treatments exhibited similar wetting regimes, all the measured and calculated parameters of ST, T1, T2, and T3 (as representative samples) were used for multivariate ordination and correlation analyses. The arithmetic average height of the roughness parameter (R_a) of the NR samples is displayed in Table 1 and AFM micrographs of NR films submitted to the different thermal treatments are displayed in Fig. 3. While there is no significant difference between ST, T1 and T2, as attested by analyses of variance (ANOVA), the thermal treatment at T3 decreases R_a. Considering the error bars in the calculated roughness parameters, the molecular rearrangement due to the thermal treatment results in a smoother surface after T3. This effect agrees with the phase transition observed during our thermal analysis (see Fig. 1**(b)** and **2(b)**), attributed to the formation of new molecular groups on the surfaces, as observed in the 1950–2100 cm^{-1} spectral region.

Hypothesizing that such chemical structural modifications affect the free energy surface-density, we calculated the solid surface energy assuming that Coulombic interactions of a permanent dipole are responsible for the polar component of a surface while the dispersive component is constituted just by van der Waals interactions. The surface energy was then calculated based on the concept of short and long-range intermolecular interactions, termed polar and dispersive interactions, respectively, and are displayed in Fig. 4**(a)**. According to the dispersive energy component, the charge fluctuations, resulting from intermolecular forces over long distances, were always more intense than the permanent dipole moments (characterized by the polar components) for all thermal treatments. The dispersive component remains stable for T1 and T2 and increases slightly for T3, indicating a higher stability of the polymeric matrix. After T3, the polar component practically vanishes. In addition, with a reduction in roughness, an increase in the contact angle for water is observed, indicating that the surface becomes more hydrophobic. Molecular rearrangements from the chemical structure modifications induced by T1 and T2 (as observed in the IR spectra displayed in Fig. 2**(c)**) affected the polar component as well, resulting in surface activation and an increase in the hydrophilicity (see contact angle values in Table 1). It is interesting to note that the decrease in the polar component of the surface energy after T3 is associated with a reduction in the roughness and a return to a hydrophobic regime.

The statistical multivariate ordination and correlation results demonstrate the main role of the polar energy components in correlation with SW (−0.95) (Supplementary **Table S3**). Considering the effects of

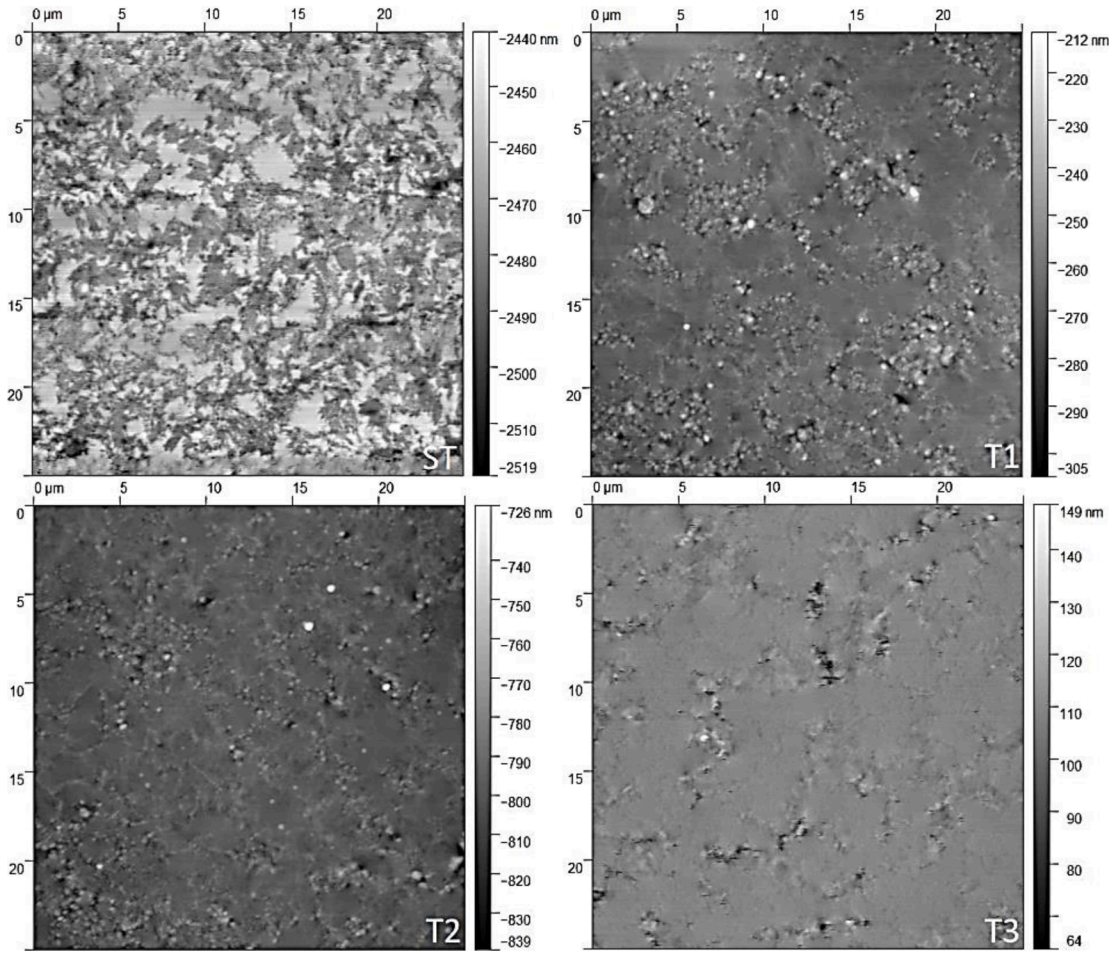

Fig. 3. AFM micrographs of NR surfaces submitted to ST, T1, T2, and T3 heat treatments.

energy components on the total energy (see the second column of values in **Table S3**), the results suggest that polar components γ^P have a fundamental role in NR surface activation, which subsequently affects SW by increasing the hydrophilicity, as evidenced by PCA. Fig. 4**(b)** shows the biplot of the PCA results with component 1 associating the loadings (green vectors) of the physicochemical parameters. This component is also responsible for 66% of statistical variance, as attested by the analysis. T1 and T2 have a noticeable influence on surface energy, in particular, due to the γ^P changes, as evidenced in the upper right quadrant of the PCA-biplot. In the same way, the increase in the γ^P decreases the contact angle, that is, it increases the hydrophilicity of the polymeric surface. The importance of these findings lies in the fact that γ^P has been pointed out as the feasibility indicator of favorable polar cell membrane-material interactions [38–40].

3.3. Cell response

Tunable SW can entail wide possibilities for the design of biomaterials, for instance, improving cell attachment on substrates for regenerative therapies. Understanding the relationship between the physicochemical modifications of the NR surface due to thermal treatments and cell-material interactions is the first step to achieve such applications. To assess the NR surface effects on cell response, Osteoblastic lineage cells MC3T3-E1 were employed, given their clinical relevance for any future biomaterial-based implant strategy (whose main applications are in bone tissues). The cell viability was increased in the presence of NR samples, compared to the control (cells cultivated on polystyrene discs), after 48 h of culture, see Fig. 5. This indicates that the NR is not toxic to osteoblasts and can even stimulate cell growth.

The effect of the thermal treatment of NR on the cell behavior was investigated with ST and T1 samples seeded at the bottom of the culture wells. The results show that simple thermal treatment of NR films at 373 K enhances SW and cell response, see Fig. 5. Due to the thermal treatment, SW increases with a contact angle decreasing from 85° to 70° for T1 (the lowest temperature of the studied thermal annealing). This finding is close to the optimized contact angles often suggested as an ideal reference measure for biomaterials [41]. It is generally believed that the cell response to a material's surface (in the absence of other intermediate adsorption layers) tends to be favored by hydrophilic regimes with contact angles within the range of 60°- 70° [42–44]. There is evidence that different wetting regimes can improve cell viability with contact angle values a little above and a little below 60° A wide wettability spectrum of titanium oxide surfaces showed an increase in cell viability with surfaces displaying contact angles within a 20°- 30° range, which was attributed to polar free-energy components that resulted from ionic interactions [39]. However, such an approach does not fit with polymeric materials, which normally exhibit hydrophobic properties and weak polar interactions. Herein, our results evidence the role of the polar interactions (quantitatively described by the parameter γ^P) in increasing surface energy and favoring polar cell membrane-material interactions in a biopolymer. The concept of polar interactions directly affecting cell viability appears to be material-dependent. Slightly ionic surfaces having a few OH^-groups available on their polymeric surfaces can be quite different from those on other biomaterials surfaces, such as ceramic coatings [45]. In this case, the charge effects are particularly relevant in affecting cell response [45–47]. From the electrostatic point of view, the increase in the polar component of the surface free energy is a result of changes in

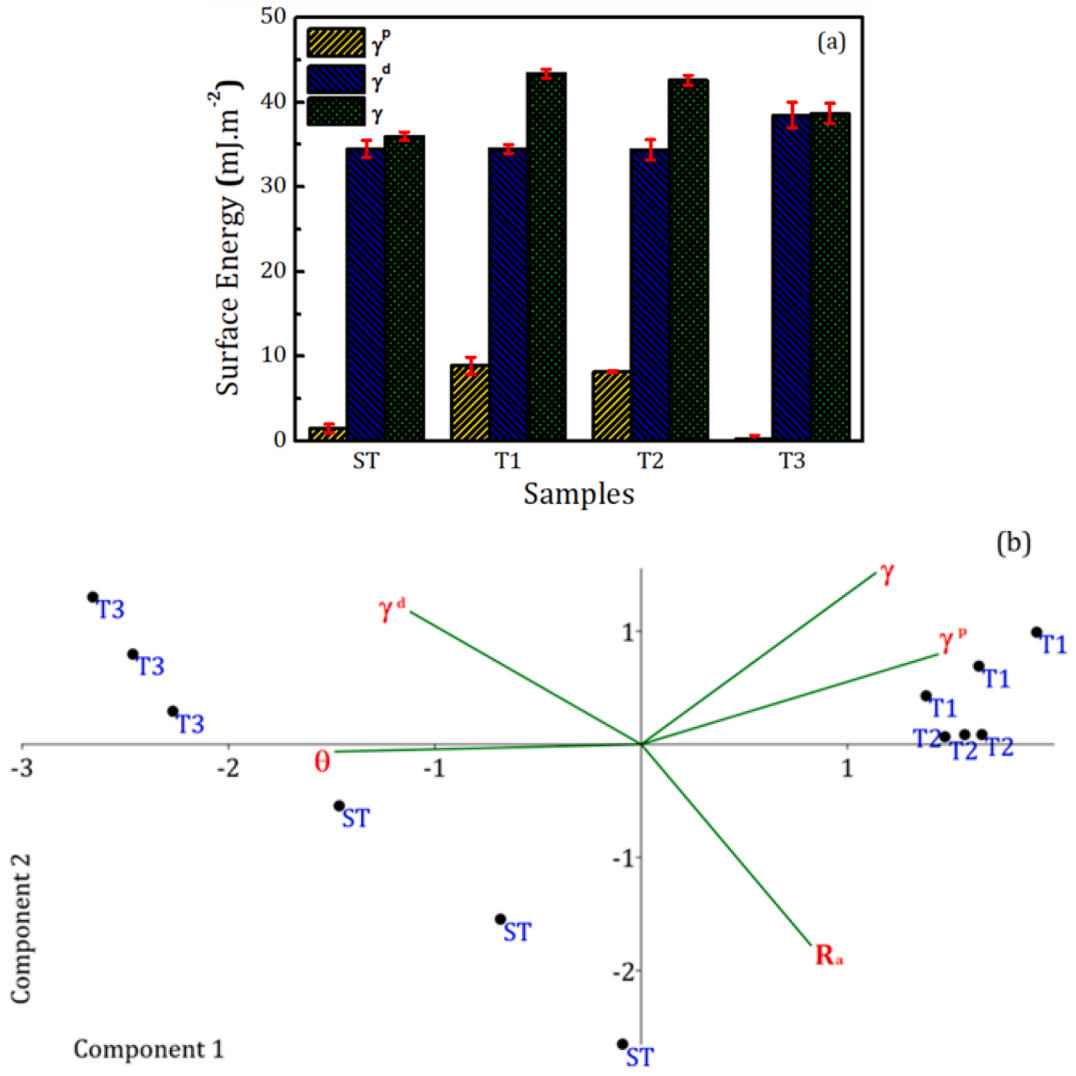

Fig. 4. Total surface free energy γ and its polar γ^p and dispersive γ^d components (with standard deviation) obtained from equilibrium contact angle measurements of the samples submitted to different thermal treatments (a), multivariate ordination by principal component analyses (PCA) for the four representative surfaces (scores, black dots) and their contributing effectors (loadings, green vectors) (b). See the Eigenvalues and Variance of the Principal Components in **Table S4**. (For interpretation of the references to colour in this figure legend, the reader is referred to the web version of this article.)

the ionic forces after molecular rearrangement, suggesting that surface charges can be induced by the treatments. These sequential events constitute a fundamental aspect in tuning the NR surface free energy, which affects SW and optimizes the cell–surface interface.

4. Conclusion

This manuscript reports the temperature effects on NR films and the possibilities of modulating their surface properties via thermal treatments to improve cell viability, tissue growth, and biocompatibility without any dopant incorporations into the NR. From a fundamental science perspective, we studied NR molecular rearrangements by in situ infrared spectroscopy with heating and cooling ramps from room-temperature up to 473 K and from room-temperature down to 80 K, respectively. The temperature changes the conformation of aromatic units, and thus modifies the structural conformation of proteins and shift the IR bands. Additionally, new molecular groups, such as C≡C and C≡N, are formed on the surfaces affecting surface free energy and interface interactions. Our results also revealed anharmonic effects that originate from the vibrational band phonons of the NR constituents. As a result of the thermal treatments, hydrophilic-hydrophobic transitions are obtained, in particular increasing the polar component of the surface free energy, which has been considered the main factor in affecting cell viability. Therefore, the wetting on the NR can be tuned by simple thermal treatments without the need of dopants. To demonstrate the potential of the temperature-tunable NR-SW in biomedical fields, we analyzed the cell response using osteoblastic cells seeded on the surfaces. Our findings show that simple thermal treatment of NR films at 373 K enhances SW and cell response, opening new horizons for applications of tunable NR-SW in biomedicine.

CRediT authorship contribution statement

Rodney Marcelo do Nascimento: Conceptualization, Methodology, Formal analysis, Investigation, Writing – original draft. **João Elias F.S. Rodrigues:** Conceptualization, Methodology, Validation, Writing – review & editing. **Bruno Z. Favarin:** Methodology, Investigation, Writing – original draft. **Ana P. Ramos:** Methodology, Investigation, Writing – original draft. **Pietro Ciancaglini:** Methodology, Investigation, Writing – original draft. **Carlos Pecharroman:** Formal analysis, Writing – review & editing. **Rachid Rahouadj:** Formal analysis, Writing – review & editing. **Antônio Carlos Hernandes:** Formal analysis, Writing – review & editing. **Ivan Helmuth Bechtold:** Validation, Formal analysis, Writing – review & editing.

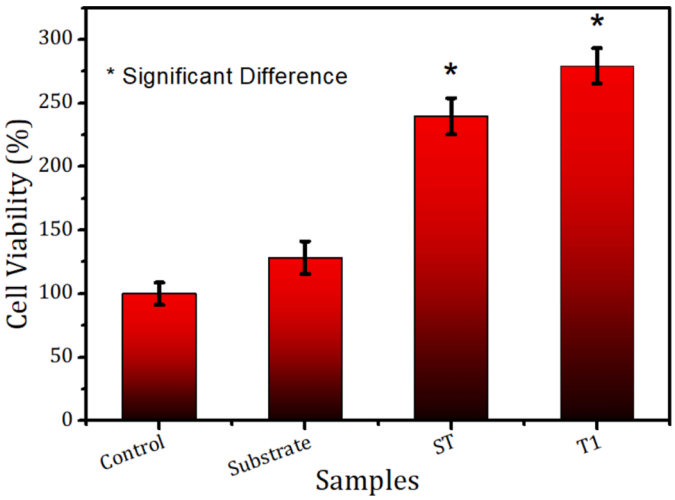

Fig. 5. Osteoblast viability after 48 h of culture on ST and T1 samples. Cells cultivated in absence of the materials (Control) and cells cultivated on polystyrene discs in absence of NR (Substrate) were used as (100% viability) control groups. (Results expressed mean ± SEM, Mann & Whitney test). * represents the significant differences between sample groups.

Declaration of Competing Interest

The authors declare that they have no known competing financial interests or personal relationships that could have appeared to influence the work reported in this paper.

Supplementary materials

Supplementary material associated with this article can be found, in the online version, at doi:10.1016/j.surfin.2022.102048.

References

[1] N.R. Barros, S.A.P. Tebonde, M.V. Cunha, R.A.M.P. Barbosa, R.D. Herculano, Highly absorptive dressing composed of natural latex loaded with alginate for exudate control and healing of diabetic wounds, Mater. Sci. Engin. 119 (2021), 111589.
[2] T. Suteewong, J. Wongpreecha, D. Polpanich, K. Jangpatarapongsa, C. Kaewsaneha, P. Tangboriboonrat, PMMA particles coated with chitosan-silver nanoparticles as a dual antibacterial modifier for natural rubber latex films, Colloids Surfaces B Bioint. 174 (2019) 544–552.
[3] G.F.B. Almeida, M.R. Cardoso, D.C. Zancanela, L.L. Bernardes, A.M.Q. Norberto, N. R. Barros, C.G. Paulino, A.L.D. Chagas, R.D. Herculano, C.R. Mendonça, Controlled drug delivery system by fs-laser micromachined biocompatible rubber latex membranes, Appl. Surf. Sci. 506 (2020), 144762.
[4] M. Furuya, N. Shimono, K. Yamazaki, R. Domura, M. Okamoto, Evaluation on cytotoxicity of natural rubber latex nanoparticles and application in bone tissue engineering, J. Soft Mater 12 (2017) 1–10.
[5] T.N. Tran, A. Nourry, G. Brotons, P. Pasetto, Antibacterial activity of natural rubber based coatings containing a new guanidinium-monomer as active agent, Prog. Org. Coatings. 128 (2019) 196–209.
[6] T.A. Dick, L.A. dos Santos, In situ synthesis and characterization of hydroxyapatite/natural rubber composites for biomedical applications, Mater. Sci. Engin. 77 (2017) 874–882.
[7] M.B. Cesar, F.A. Borges, A.P. Bilck, F. Yamashita, C.G. Paulino, R.D. Herculano, Development and characterization of natural rubber latex and polylactic acid membranes for biomedical application, J. Polym. Environ. 28 (2020) 220–230.
[8] M.H. Azarian, P. Boochathum, M. Kongsema, Biocompatibility and biodegradability of filler encapsulated chloroacetated natural rubber/polyvinyl alcohol nanofiber for wound dressing, Mater. Sci. Engin. 103 (2019), 109829.
[9] D.C. Zancanela, C.S. Funari, R.D. Herculano, V.M. Mello, C.M. Rodrigues, F. A. Borges, N.R. de Barros, C.M. Marcos, A.M.F. Almeida, A.C. Guastaldia, Natural rubber latex membranes incorporated with three different types of propolis: physical-chemistry and antimicrobial behaviours, Mater. Sci. Engin. 97 (2019) 576–582.
[10] R.O. Medupin, O.K. Abubakre, A.S. Abdulkareem, R.A. Muriana, A. S. Abdulrahman, Carbon nanotube reinforced natural rubber nanocomposite for anthropomorphic prosthetic foot purpose, Sci. Rep. 9 (2019) 20146.
[11] R.M. Nascimento, F.L. Faita, D.L.S. Agostini, A.E. Job, F.E.G. Guimarães, I. H. Bechtold, Production and characterization of natural rubber-Ca/P blends for biomedical purposes, Mater. Sci. Engin. 39 (2014) 29–34.
[12] R.M. do Nascimento, A.J. de Paula, N.C. Oliveira, A.C. Alves, Y.M.L.O. Aquino, A. G.S. Filho, J.E.F.S. Rodrigues, A.C. Hernandes, Towards the production of natural rubber-calcium phosphate hybrid for applications as bioactive coatings, Mater. Sci. Engin. 94 (2019) 417–425.
[13] M. Kinoshita, Y. Okamoto, M. Furuya, M. Okamoto, Biocomposites composed of natural rubber latex and cartilage tissue derived from human mesenchymal stem cells, Mater. Today Chem. 12 (2019) 315–323.
[14] R.M. Do Nascimento, S.M.M. Ramos, I.H. Bechtold, A.C. Hernandes, Wettability Study on Natural Rubber Surfaces for Applications as Biomembranes, ACS Biomater. Sci. Eng. 4 (2018) 2784–2793.
[15] R.M. do Nascimento, J.F. Schmitt, U. Sarig, J.E.F.S. Rodrigues, C. Pecharromán, A. P. Ramos, P. Ciancaglini, F.L. Faita, R. Rahouadj, A.C. Hernandes, I.H. Bechtold, Surface wettability of a natural rubber composite under stretching: a model to predict cell survival, Langmuir 15 (2021) 4639–4646.
[16] N.B. Guerra, G.S. Pegorin, M.H. Boratto, N.R. de Barros, C.F.O. Graeff, R. D. Herculano, Biomedical applications of natural rubber latex from the rubber tree Hevea brasiliensis, Mater. Sci. Engin. 126 (2021), 112126.
[17] J.H. Park, C.E. Wasilewski, N. Almodovar, R. Olivares-Navarrete, B.D. Boyan, R. Tannenbaum, Z. Schwartz, The responses to surface wettability gradients induced by chitosan nanofilms on microtextured titanium mediated by specific integrin receptors, Biomaterials 33 (2012) 7386–7393.
[18] S.A. Shabalovskaya, D. Siegismund, E. Heurich, M. Rettenmayr, Evaluation of wettability and surface energy of native Nitinol surfaces in relation to hemocompatibility, Mater. Sci. Engin. 33 (2013) 127–132.
[19] R.A. Gittens, L. Scheideler, F. Rupp, S.L. Hyzy, J. Geis-Gerstorfer, Z. Schwartz, B. D. Boyan, A review on the wettability of dental implant surfaces II: biological and clinical aspects, Acta Biomater. 10 (2014) 2907–2918.
[20] A.O. Ijaola, E.A. Bamidele, C, J.Akisin, I.T. Bello, A.T. Oyatobo, A. Abdulkareem, P. K. Farayibi, E. Asmatulu, Wettability transition for laser textured surfaces: a comprehensive review. Surf. Interf., Volume 21, December 2020, 100802.
[21] S. Rbihi, A. Aboulouard, L. Laallam, A. Jouaiti, Contact angle measurements of cellulose based thin film composites: wettability, surface free energy and surface hardness, Surf. Interf. 21 (2020), 100708.
[22] C.C. Ho, M.C. Khew, Surface free energy analysis of natural and modified natural rubber latex films by contact angle method, Langmuir 16 (2000) 1407–1414.
[23] D. Rana B. M. Mandal S. N. Bhattacharyya, Miscibility and phase diagrams of poly (phenyl acrylate) and poly(styrene-co-acrylonitrile) blends, Polymer (Guildf) 34 (7) (1993) 1454–1459.
[24] Y. Song, Y. Liu, H. Jiang, S. Li, C. Kaya, T. Stegmaier, Z. Han, L. Ren, Temperature-tunable wettability on a bioinspired structured graphene surface for fog collection and unidirectional transport, Nanoscale 10 (8) (2018) 3813–3822.
[25] J. Mosnáček, A. Popelka, J. Osicka, J. Filip, M. Ilcikova, J. Kollar, A. Yousaf, T. Bertok, J. Tkac, P. Kasak, Modulation of wettability, gradient and adhesion on self-assembled monolayer by counterion exchange and pH, J. Colloid Interface Sci. 512 (2018) 511–521.
[26] Y. Bai, F. Zhang, K. Xu, X. Wang, C. Wang, H. Zhang, Y. Tan, P. Wang, Pickering emulsion strategy to control surface wettability of polymer microspheres for oil–water separation, Appl. Surf. Sci. 566 (2021), 150742.
[27] D. Hill, A. Barron, S. Alexander, Controlling the wettability of plastic by thermally embedding coated aluminium oxide nanoparticles into the surface, J. Colloid Interface Sci. 567 (2020) 45–53.
[28] O. Ryabkova, L. Redina, E. Salomatina, L. Smirnova, Hydrophobizated poly (titanium oxide) containing polymeric surfaces with UV-induced reversible wettability and self-cleaning properties, Surf. Interf. 18 (2020), 100452.
[29] Q. Wang, H. Wang, Z. Zhu, N. Xiang, Z. Wang, G. Sun, Switchable wettability control of titanium via facile nanosecond laser-based surface texturing, Surf. Interf. 24 (2021), 101122.
[30] D.K. Owens, R.C. Wendt, Estimation of the surface free energy of polymers, J. Appl. Polym. Sci. 13 (1969) 1741–1747.
[31] A.E.M. Cruz, B.C. Tovani, B.Z. Favarin, P.R.M. Soares, Y.S. Fukuda, P. Ciancaglini, A.P. Ramos, Syntesis of Sr-morin complex and its in vitro response: decrease in osteoclast differentiation while sustaining osteoblast mineralization ability, J. Mater. Chem. B 7 (2019) 823.
[32] J.E. Jackson, A. Hoboken, User's Guide to Principal Components Analysis, John Wiley&Sons, NJ, 2003.
[33] S. Rolere, S. Liengprayoon, L. Vayssea, J. Sainte-Beuvea, F. Bonfisa, Investigating natural rubber composition with fourier transform infrared (FT-IR) spectroscopy: a rapid and non-destructive method to determine both protein and lipid contents simultaneously, Polym. Test. 43 (2015) 83–93.
[34] F. Lhert, F. Capelle, D. Blaudez, C. Heywang, J. Turlet, Raman spectroscopy of phospholipid black fims, Phys. Chem. B. 104 (2000) 11704–11707.
[35] A. Rygul, K. Majzner, K.M. Marzec, A. Kaczor, M. Pilarczyk, M. Baranska, Raman spectroscopy of proteins: a review, J. Raman Spectrosc. 44 (2013) 1061–1076.
[36] M. Balkanski, R. Wallis, E. Haro, Anharmonic effects in light scattering due to optical phonons in silicon, Phys. Rev. B. 28 (1983) 1928–1934.
[37] S. Nuntang, S. Yousatit, T. Yokoi, C. Ngamcharussrivichai, Tunable mesoporosity and hydrophobicity of natural rubber/hexagonal mesoporous silica nanocomposites, Microporous Mesoporous Mater. 275 (2019) 235–243.
[38] A. Garcia, H. Zou, K.R. Hossain, Q.H. Xu, A. Buda, R.J. Clarke, Polar interactions play an important role in the energetics of the main phase transition of phosphatidylcholine membranes, ACS Omega 4 (2019) 518–527.

[39] R.M. do Nascimento, U. Sarig, N.C. da Cruz, V.R. de Carvalho, C. Eyssartier, L. Siad, J.F. Ganghoffer, A.C. Hernandes, R. Rahouadj, Optimized-surface wettability: a new experimental 3D modeling approach, Adv. Theory Simul. 2 (2019), 1900079.
[40] D. Yongabi, M. Khorshid, A. Gennaro, S. Jooken, S. Duwé, O. Deschaume, P. Losada-Pérez, P. Dedecker, C. Bartic, M. Wübbenhorst, P. Wagner, QCM-D study of time-resolved cell adhesion and detachment: effect of surface free energy on eukaryotes and prokaryotes, ACS Appl. Mater. Interfaces 12 (2020) 18258–18272.
[41] M.M. Gentleman, E. Gentleman, The role of surface free energy in osteoblast–biomaterial interactions, Int. Mater. Rev. 59 (2014) 417–429, 8.
[42] T. Groth, G. Altankov, Studies on cell-biomaterial interaction: role of tyrosine phosphorylation during fibroblast spreading on surfaces varying in wettability, Biomaterials 12 (1996) 1227–1234.
[43] J.M. Schakenraad, H.J. Busscher, C.R. Wildevuur, J. Arends, Thermodynamic aspects of cell spreading on solid substrata, Cell Biophys. 1 (1988) 75–91.
[44] Y. Tamada, Y. Ikada, Fibroblast growth on polymer surfaces and biosynthesis of collagen, J. Biomed. Mater. Res. 7 (1994) 783–789.
[45] R.M. do Nascimento, V.R. Carvalho, J.S. Govone, A.C. Hernandes, N.C. Cruz, Effects of negatively and positively charged Ti metal surfaces on ceramic coating adhesion and cell response, J. Mater. Sci. Mater. Med. 28 (2017) 33.
[46] M. Nakamura, A. Nagai, T. Hentunen, J. Salonen, Y. Sekijima, T. Okura, K. Hashimoto, Y. Toda, H. Monma, K. Yamashita, Surface electric fields increase osteoblast adhesion through improved wettability on hydroxyapatite electret, ACS Appl. Mater. Interfaces 10 (2009) 2181–2189.
[47] K. Xiao, Y. Li, J. Luo, J.S. Lee, W. Xiao, A.M. Gonik, R.G. Agarwal, K.S. Lam, The effect of surface charge on in vivo biodistribution of PEG-oligocholic acid based micellar nanoparticles, Biomaterials 32 (2011) 3435–3446.